Quantum Master Equation Approach to the Second Hyperpolarizability of Nanostar Dendritic Systems

Masayoshi Nakano,*,† Ryohei Kishi,† Nozomi Nakagawa,† Tomoshige Nitta,† and Kizashi Yamaguchi‡

Division of Chemical Engineering, Department of Materials Engineering Science, Graduate School of Engineering Science, Osaka University, Toyonaka, Osaka 560-8531, Japan, and Department of Chemistry, Graduate School of Science, Osaka University, Toyonaka, Osaka 560-0043, Japan

Received: November 27, 2004; In Final Form: March 3, 2005

We investigate the dynamic second hyperpolarizability (γ) of nanostar dendritic systems using the quantum master equation approach. In the nanostar dendritic systems composed of three-state monomers, the multistep exciton states are obtained by the dipole−dipole interactions, and the directional energy transport, i.e., exciton migration, from the periphery to the core is predicted to occur by the relaxation between exciton states originating in the exciton−phonon coupling. The effects of the intermolcecular interaction and the exciton migration, i.e., exciton relaxation, on the γ in the third-harmonic generation (THG) are examined in the three-photon off- and on- resonance regions using the two-exciton model. Furthermore, the method for analysis of spatial contributions of excitons to γ is presented by partitioning the total γ into the one- and two-exciton contributions. It turns out that the exciton relaxation between exciton states causes significant broadening of the spectra of γ and their mutual overlap as well as the relative increase of two-exciton contributions in the nanostar dendritic system.

1. Introduction

Excitation energy transport is one of the essential processes in photosynthesis in green plants on earth and also finds an important application in photonics and biology.[1−4] In particular, the electron-transfer and energy-transfer processes in π-conjugated oligomers and polymers have attracted much attention in view of organics-based materials including nonlinear optical properties and semiconducting properties and have been actively investigated, for example, by the groups of Brédas and Marder.[5−9] The efficient and controllable energy transport is known to be one of the fascinating properties of dendritic systems with ordered fractal-like architecture, which exhibits a directed, multistep energy transport of absorbed light. There have been lots of studies on the efficient light-harvesting properties of phenylacetylene dendrimers and dendritic aggregates with a fractal-antenna (Cayley-tree) structure.[10−20] It has been found that the efficient energy transport is carried out by the multistep exciton migration from the periphery to the core, and is related to two peculiar structural features: (I) increase in the lengths of linear-legs involved in each generation as going from the periphery to the core and (II) meta-branching points (meta-substituted benzene rings). These features are predicted to provide multistep exciton states, in which the exciton distribution is spatially well localized in each generation and the exciton energy decreases as going from the periphery to the core region.[21−28] In our previous studies using the dipole-coupled dendritic aggregate models,[29−31] we have also pointed out the necessity of the relaxation effect between exciton states, originating in exciton−phonon coupling, for such efficient exciton migration in addition to multistep exciton states. The efficient multistep relaxation turns out to require partial spatial overlaps of exciton distributions between neighboring exciton states, which are respectively distributed in adjacent generations linked with meta-branching points. Our treatment has been extended and applied to real dendrimeric molecules based on the ab initio molecular orbital (MO) configuration interaction (CI) calculations.[32] As a result, structural features I and II are found to satisfy these two conditions: (A) a well-segmented exciton distribution in each multistep exciton state and (B) the existence of partial overlaps of exciton distributions between neighboring exciton states, to realize efficient directed multistep exciton migration.

In this study, we examine the second hyperpolarizability (γ) in the third harmonic generation (THG) of an associated dendrimer derivative, "nanostar", terminated at the focal point with a core monomer, e.g., a perylene luminophor. This compound exhibits efficient energy transport to the core monomer, which eventually emits the fluorescence enormously enhanced as compared to the case of isolated core monomer. We here develop a calculation scheme of dynamic $\gamma(-3\omega;\omega,\omega,\omega)$ for such dendritic nanostar systems including the dipole−dipole interaction and exciton relaxation effects using the two-exciton dipole-coupled aggregate model with the nanostar structure composed of three state monomers. The relaxation between exciton states is taken into account in the quantum master equation approach including weak exciton−phonon coupling. We also present a method for analysis of the spatial contribution of one- and two-exciton generation to γ using the density matrix formula. On the basis of the present results, we discuss the effects of the multistep exciton states, which is generated by the intermolecular dipole−dipole interaction, and the exciton relaxation between them on the γ(THG) spectrum.

* Corresponding author. E-mail: mnaka@cheng.es.osaka-u.ac.jp.

† Division of Chemical Engineering, Department of Materials Engineering Science, Graduate School of Engineering Science, Osaka University.

‡ Department of Chemistry, Graduate School of Science, Osaka University.

10.1021/jp044599r CCC: $30.25
Published on Web 04/02/2005

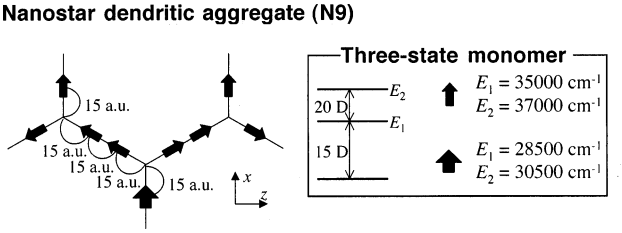

Figure 1. Structure of a nanostar dendritic aggregate model composed of two kinds of monomers.

2. Methodology

2.1. Model Hamiltonian of Molecular Aggregate. We consider a molecular aggregate (Figure 1) composed of three-state monomers with excitation energies $\{E^k_{i_k}\}$ and magnitudes of transition moments $\{\mu^k_{i_k,i'_k}\}$ ($k = 1, 2, ..., N$, N: the number of monomers; $i_k = 1$, 2 and 3). The monomer is approximated to be a dipole. This approximation is considered to be acceptable if the intermolecular distance (R_{kl}) is larger than the size of a monomer. For two dipoles k and l, the angle between a dipole $k(l)$ and a line drawn from the dipole site k to l is $\theta_{k_l}(\theta_{l_k})$. The Hamiltonian, H_S, for the molecular aggregate is expressed in atomic units by

$$H_S = \sum_k^N \sum_{i_k}^3 E^k_{i_k} a^+_{i_k} a_{i_k} + \frac{1}{4\pi\epsilon_0} \sum_{k<l}^N \sum_{\substack{i_k,i'_k,\\ i_l,i'_l}}^3 \mu^k_{i_k i'_k} \mu^l_{i_l i'_l} [(\cos(\theta_{k_l} - \theta_{l_k}) - 3\cos\theta_{k_l}\cos\theta_{l_k})/R^3_{kl}] a^+_{i_k} a_{i'_k} a^+_{i_l} a_{i'_l} \quad (1)$$

where the first and the second terms represent a noninteracting Hamiltonian and a dipole−dipole interaction, respectively. The $a^+_{i_k}$ and $a_{i'_k}$ represent respectively the creation and annihilation operators for the i_k state of monomer k. The matrix elements of H_S in the basis for the aggregate $\{|\varphi^1_{i_1}\varphi^2_{i_2}...\varphi^N_{i_N}\rangle\}$, which is constructed from a direct product of a state vector for each monomer $\{|\varphi^k_{i_k}\rangle\}$, are presented in our previous paper.[29−31] By diagonalizing the Hamiltonian matrix H_S (eq 1), we can obtain eigenenergies $\{E_\alpha\}$ and eigenstates $\{|\alpha\rangle\}$ ($a = 1, ..., M$), where M is the size of the basis used. The M is $1 + {}_NC_1 + {}_NC_2$ in the present study since we consider a two-exciton model, which is at least necessary for describing the third-order nonlinear optical processes. The transition dipole matrix elements ($\mu_{\alpha\beta}$) in the direction of applied field for this new state model are also calculated.[29−31] It is noted that the transition moments between the ground and one-exciton states, those between one-exciton states, and those between one- and two-exciton states, only exist in the present model.

2.2. Density Matrix Formalism for a Molecular Aggregate Interacting with Time-Dependent Electric Fields. One- and two-excitons represented by aggregate basis $\{|i\rangle\} \equiv \{|\varphi^1_{i_1}\varphi^2_{i_2}...\varphi^N_{i_N}\rangle\}$ ($2 \le i \le 1 + {}_NC_1 + {}_NC_2$) are assumed to interact with a nuclear vibration, i.e., a phonon state $\{|q_i\rangle\}$ with a frequency $\{\Omega_{q_i}\}$. The Hamiltonian, H_R, for the phonon is given by

$$H_R = \sum_i^M \sum_{q_i} \Omega_{q_i} c^+_{i,q_i} c_{i,q_i} \quad (2)$$

where c^+_{i,q_i} and c_{i,q_i} represent the creation and annihilation operators concerning a phonon state $|q_i\rangle$, respectively. The interaction Hamiltonian, H_{SR}, for weak exciton−phonon coupling is assumed to be

$$H_{SR} = \sum_i^M \sum_{q_i} |i\rangle\langle i|(\kappa^*_{i,q_i} c^+_{i,q_i} + \kappa_{i,q_i} c_{i,q_i}) \quad (3)$$

where κ_{i,q_i} denotes a coupling constant between the exciton represented by basis $|i\rangle$ and a phonon state $|q_i\rangle$. We investigate the dynamics of exciton system involved in total system composed of exciton (H_S), phonon (H_R), exciton−phonon interaction (H_{SR}) and the interaction between exciton and external electric field F (H_{int}). Using the standard method of relaxation theory,[33] we obtain a quantum master equation[29−32] for exciton density matrix ρ under the Born−Markov approximation:

$$\dot\rho_{\alpha\alpha} = -\sum_m^M \Gamma_{\alpha\alpha;mm}\rho_{mm} - F\sum_n^M(\mu_{\alpha n}\rho_{n\alpha} - \rho_{\alpha n}\mu_{n\alpha}) \quad (4)$$

and

$$\dot\rho_{\alpha\beta} = -i(\omega_\alpha - \omega_\beta)\rho_{\alpha\beta} - \sum_{m,n}^M \Gamma_{\alpha\beta;mn}\rho_{mn}.(\alpha \neq \beta) \quad (5)$$

The relaxation factors are expressed by

$$\Gamma_{\alpha\alpha;mm} = 2\delta_{\alpha m}\sum_k^M\sum_i^N |C_{i\alpha}|^2|C_{ik}|^2\gamma_i(\omega_m - \omega_k) - 2\sum_i^N |C_{i\alpha}|^2|C_{im}|^2\gamma_i(\omega_m - \omega_\alpha) \quad (6)$$

and

$$\Gamma_{\alpha\beta;mn} = \sum_k^M\sum_i^N [\delta_{\beta n}C^*_{i\alpha}|C_{ik}|^2C_{im}\gamma_i(\omega_m - \omega_k) + \delta_{\alpha m}C^*_{in}|C_{ik}|^2C_{i\beta}\gamma_i(\omega_n - \omega_k)] - \sum_i^N [C^*_{i\alpha}C_{im}C^*_{in}C_{i\beta}\{\gamma_i(\omega_m - \omega_\alpha) + \gamma_i(\omega_n - \omega_\beta)\}] \quad (7)$$

where

$$\gamma_i(\omega) = \frac{2g_i}{1 + \exp(-\omega/k_BT)} \quad (8)$$

This factor $\gamma_i(\omega)$ is taken to satisfy the thermal equilibrium condition: g_i indicates the high-temperature limit of $\gamma_i(\omega)$, and k_B is the Boltzmann constant. We solve eqs 4 and 5 numerically using the fourth-order Runge−Kutta method.

Using the definition of nonperturbative (hyper)polarizabilities,[34] we can obtain the $\gamma(-3\omega;\omega,\omega,\omega)$ in the THG as

$$\gamma(-3\omega;\omega,\omega,\omega) = \frac{\boldsymbol{p}(3\omega)}{27\epsilon^3(\omega)} \quad (9)$$

where $\boldsymbol{p}(3\omega)$ is obtained by the Fourier transformation of induced polarization time series. The γ value (complex quantity) is also described by the Fourier transformation of real parts of density matrices $\rho^{real}_{ba}(t)$ in the aggregate basis ($\{|a\rangle\} \equiv \{|\varphi^1_{i_1}\varphi^2_{i_2}...\varphi^N_{i_N}\rangle\}$):

$$\gamma(-3\omega;\omega,\omega,\omega) = \sum_{a>b}^M \gamma_{a-b} = \sum_{a>b}^M \frac{2\mu_{ab}\rho^{real}_{ba}(3\omega)}{27\epsilon^3(\omega)} \quad (10)$$

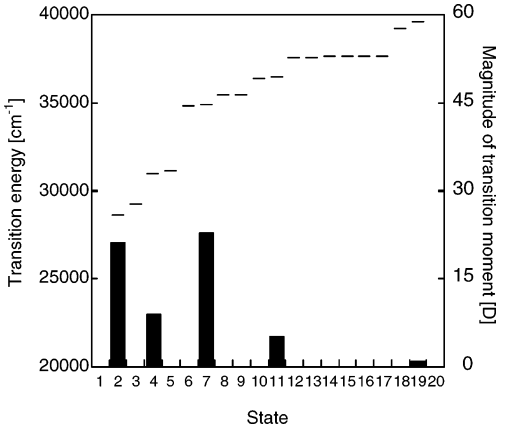

Figure 2. One-exciton state energies E_{l1} [cm^{-1}] (l = 2, ..., 19) and the magnitude of transition moments μ_{l1} [D] between the ground (1) and exciton (l) states of the dendritic aggregate shown in Figure 1.

In the two-exciton model, the μ_{ab} exists between the $|11...1\rangle$ (1: the ground state of monomer) and one-exciton states, e.g., $|12...1\rangle$ (2: the first excited state of monomer), or between one exciton states, e.g., $|121...1\rangle$ and $|131...1\rangle$ (2 and 3 indicate the first and the second excited states of monomer, respectively), or between one- and two-exciton states, e.g., $|12111...1\rangle$ and $|13121...1\rangle$, so that the γ_{a-b} represents the contribution to γ of the virtual one- or two-exciton generation represented by a basis pair *a*-*b*. We can elucidate the spatial contribution of γ_{a-b} by plotting its value on the sites with newly generated exciton distribution represented by bases *a* and *b*. In this study, we represent the spatial contributions of one- and two-exciton generations to γ by summing up the γ_{a-b} concerning one- or two-exciton basis *a* (*b*) on each unit site. For example, in the case of $a = |12111...1\rangle$ and $b = |12121...1\rangle$, we can elucidate the spatial contribution of two-exciton generation to γ by showing this distribution γ_{a-b} on the fourth monomer, in which the second exciton generates with respect to the basis *a*.

3. Results and Discussion

3.1. Exciton Migration under External Oscillating Electric Field. To investigate the relation between the exciton relaxation and dynamic γ values, we first examine the exciton migration in the nanostar dendritic system (Figure 1) under the external oscillating electric field. The present nanostar dendritic aggregate model is composed of two types of three-state monomers: the first type is the monomer in dendron parts, i.e., leg regions, with excitation energies (E_{21} = 35 000 cm^{-1} and E_{31} = 37 000 cm^{-1}) and transition moments (μ_{21} = 15 D and μ_{32} = 20 D), while the second type is the monomer in core region with excitation energies (E_{21} = 28 500 cm^{-1} and E_{31} = 30 500 cm^{-1}) and transition moments (μ_{21} = 15 D and μ_{32} = 20 D). The lower-lying excitaed states in the core monomer as compared to those of other monomers in dendoron parts mimic the energy acceptor group in real nanostar dendrimers.[20,23] The feature that the intermolecular distance ($15\sqrt{3}$ a.u.) between neighboring monomers through branching points is larger than that (15 au) in the linear-leg region corresponds to the well decoupling of π-conjugation at the meta-substituted benzene rings in real phenylacetylene dendrimers.[26−32]

Figure 2 shows low-lying one-exciton states obtained by diagonalizing two-exciton model Hamiltonian (eq 1) and transition moments between the ground state and the exciton state. Because of the intermolecular interaction between monomers, a multistep structure is observed in the exciton states (Figure 2), whose dominant exciton distribution region is changed from the periphery to the core as going from the high-lying (**7**) to low-lying (**2**) exciton states with transition moments from the ground state.

TABLE 1: Relative Relaxation Factors $\Delta\gamma_{\alpha\beta}$ [cm^{-1}] for Models I (a), II (b), and III (c)

β	$\alpha = 7$	$\alpha = 6$	$\alpha = 5$	$\alpha = 4$	$\alpha = 3$	$\alpha = 2$
			(a) g_i = 0 cm^{-1}			
6	0.00					
5	0.00	0.00				
4	0.00	0.00	0.00			
3	0.00	0.00	0.00	0.00		
2	0.00	0.00	0.00	0.00	0.00	
1	35.00	35.00	35.00	35.00	35.00	35.00
			(b) g_i = 200 cm^{-1}			
6	11.70					
5	0.00	0.00				
4	4.24	4.24	0.00			
3	3.83	3.83	0.00	143.12		
2	0.64	0.64	0.00	152.76	33.27	
1	35.00	35.00	35.00	35.00	35.00	35.00
			(c) g_i = 1000 cm^{-1}			
6	58.49					
5	0.00	0.00				
4	21.22	21.22	0.00			
3	19.13	19.13	0.00	715.58		
2	3.22	3.22	0.00	763.80	166.34	
1	35.00	35.00	35.00	35.00	35.00	35.00

To elucidate the time evolution of exciton population, we numerically solve eq 4 using the initially populated state **7** with exciton distribution in the periphery region. The applied electric field is resonant with the exciton state **7** (ω = 34 885 cm^{-1}) and the population damping factor from the exciton states to the ground state is fixed to γ_{i0} = 35 cm^{-1} for all the models. The exciton relaxation rates are calculated by eq 6, and reflect the relative exciton distribution, energy gap between exciton states, and external bath temperature. The only parameter is g_i, which is the high-temperature limit of $\gamma_i(\omega)$ (eq 8). We examine three types of exciton relaxation cases by changing g_i: model I is the nonexciton relaxation case with g_i = 0 cm^{-1}, model II is the case with g_i = 200 cm^{-1}, which gives smaller relaxation factors between exciton states than the damping to the ground state, i.e., exciton annihilation, (γ_{i0}) from each exciton state and model III is the case with g_i = 1000 cm^{-1}, which gives larger relaxation factors between exciton states than γ_{i0}. Table 1 gives relative relaxation factors $\Delta\gamma_{\alpha\beta}$[30] for these models calculated by

$$\Delta\gamma_{\alpha\beta} = 2\sum_{i}^{N}|C_{i\alpha}|^2|C_{i\beta}|^2\{\gamma_i(\omega_\alpha - \omega_\beta) - \gamma_i(\omega_\beta - \omega_\alpha)\} \quad (11)$$

where positive $\Delta\gamma_{\alpha\beta}$ represents the relaxation rate from state α to β, while negative $\Delta\gamma_{\alpha\beta}$ does the opposite relaxation. From the relative relaxation factors for these models, the most contributed exciton relaxation pathways except for the ground state is shown to be **7** → **6** → **4** (**3**) → **2** and **7** → **6** → **4** → **3** → **2**, which represent the exciton migration from the periphery to the core. The variation in exciton population under the external oscillating electric field (100 MW/cm^2, $\hbar\omega = E_{71}$) is shown in Figure 3. As expected, model I (Figure 3a) exhibits an exponentially decaying Rabi oscillation between state **7** and the ground state (**1**), while in models II (Figure 3b) and III (Figure 3c) Rabi oscillations disappear and alternatively the increase in the exciton population in lower-lying exciton states appears, the feature of which originates in the exciton migration from high-lying to low-lying states. Although in model II the stationary exciton population in the periphery region (states **6**

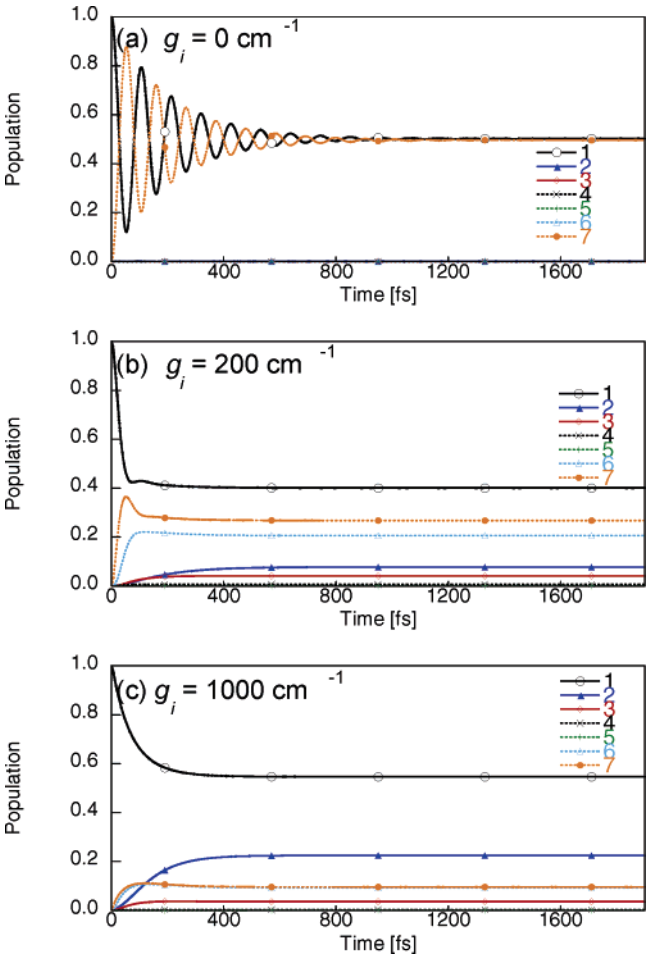

Figure 3. Variation in populations of exciton states for model I (g_i = 0 cm^{-1}) (a), II (g_i = 200 cm^{-1}) (b), and III (g_i = 1000 cm^{-1}) (c) under an external oscillating electric field with frequency (34885 cm^{-1}) and power (100 MW/cm^2).

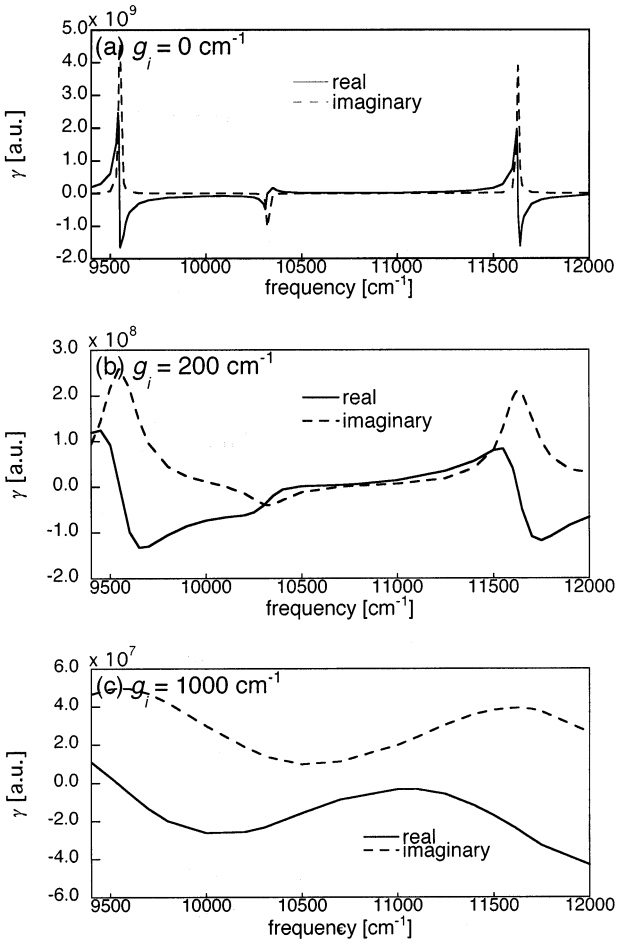

Figure 4. Real and imaginary γ (THG) spectra in the three-photon on- and off- resonance regions for models I (a), II (b), and III (c). The first, second and third imaginary peaks correspond to the three-photon resonances of $E_{21}/3$ (≅9547 cm^{-1}), $E_{41}/3$ (≅10319 cm^{-1}), and $E_{71}/3$ (≅11628 cm^{-1}), respectively.

and **7**) is still larger than that in the intermediate and core regions (states **3** and **2**), in model III the exciton population in the core monomer (state **2**) is larger than that in the intermediate and periphery regions (states **3** and **7**), indicating the significant exciton migration from the periphery to the core even under oscillating electric field.

3.2. THG Spectra of Nanostar Dendritic Systems. Figure 4 shows the real and imaginary γ spectra of THG for (a) model I (g_i = 0 cm^{-1}), (b) model II (g_i = 200 cm^{-1}), and (c) model III (g_i = 1000 cm^{-1}) in the three-photon off- and on-resonant regions with respect to low-lying one-exciton states. For the noninteracting case, the resonance peak appears in the three photon resonance region for the core monomer ($E_{21}^{\text{core}}/3$ = 28500/3 = 9500 cm^{-1}) and that ($E_{21}^{\text{dendron}}/3$ = 35000/3 ≈ 11666.67 cm^{-1}) for monomers in dendron parts. On the other hand, for interacting models I, II, and III, the energy levels are mutually split by the dipole−dipole interaction, so that three kinds of three-photon resonance peaks concerning states **7** (E_{71} = 34 885 cm^{-1}), **4** (E_{41} = 30 958 cm^{-1}) and **2** (E_{21} = 28 640 cm^{-1}) (see Figure 2) appear. Therefore, the first change of THG spectrum by constructing nanostar dendritic aggregate is the displacement of the resonance peak positions by splitting the energy levels due to the dipole−dipole interaction.

The second change appears in the broadening of spectral peaks, which is caused by the exciton relaxation. There are three kinds of relaxation factors: the population damping to the ground state (γ_{i0} = 35 cm^{-1} for all exciton states in all models), the diagonal exciton relaxation (eq 6), i.e., exciton migration, and the off-diagonal exciton relaxation (eq 7). For model I (Figure 4a), since only the small damping to the ground state exists, the THG peaks are relatively sharp, and the relative peak intensity is determined by the relative magnitude of transition moments. In contrast, the peak intensities in models II (Figure 4b) and III (Figure 4c) are shown to be remarkably reduced than those in model I, and significant broadening occurs in models II and III. These features can be understood by the relative magnitude of off-diagonal exciton relaxations in models I, II, and III. Since the high-temperature limit g_i contributes to the magnitude of exciton relaxation factors, the exciton relaxation effects in model III is larger than that in model II. It is noted that the off-diagonal exciton relaxation factor including pure relaxation factors, which gives a dominant contribution in the off-diagonal exciton relaxation (eq 7), are much larger than the diagonal exciton relaxation factor, i.e., exciton migration rate (eq 6). From the relation between eq 6 and the feeding parameter $\gamma_{\alpha\beta}$, which is an inelastic transition rate from α to β, we obtain

$$\gamma_{\alpha\beta} = 2\sum_{i}^{N} |C_{i\alpha}|^2 |C_{i\beta}|^2 \gamma_i(\omega_\alpha - \omega_\beta) \qquad (12)$$

The dominant diagonal part of off-diagnoal relaxation factor (eq 7), i.e., $\Gamma_{\alpha\beta;\alpha\beta}$, is expressed as

$$\Gamma_{\alpha\beta;\alpha\beta} = \sum_{k}^{M}\sum_{i}^{N}[|C_{i\alpha}|^2|C_{ik}|^2\gamma_i(\omega_\alpha - \omega_k) + |C_{i\beta}|^2|C_{ik}|^2\gamma_i(\omega_\beta - \omega_k)] - 2\sum_{i}^{N}|C_{i\alpha}|^2|C_{i\beta}|^2\gamma_i(0) \quad (13)$$

This factor is composed of off-diagnoal part ($\Gamma_{\alpha\beta} = (\Gamma_{\alpha\alpha} + \Gamma_{\beta\beta})/2$) originating in the diagonal relaxation factor:

$$\Gamma_{\alpha\alpha} = \sum_{k(\neq\alpha)}^{M}\gamma_{\alpha k} = 2\sum_{k(\neq\alpha)}^{M}\sum_{i}^{N}|C_{i\alpha}|^2|C_{ik}|^2\gamma_i(\omega_\alpha - \omega_k) \quad (14)$$

and the pure dephasing part $\Gamma'_{\alpha\beta;\alpha\beta}$, so that we can obtain the expression of pure dephasing part as

$$\begin{aligned}\Gamma'_{\alpha\beta} &= \Gamma_{\alpha\beta;\alpha\beta} - \Gamma_{\alpha\beta} \\ &= \sum_{i}^{N}|C_{i\alpha}|^4\gamma_i(0) + \sum_{i}^{N}|C_{i\beta}|^4\gamma_i(0) - 2\sum_{i}^{N}|C_{i\alpha}|^2|C_{ik}|^2\gamma_i(0) \\ &= \sum_{i}^{N}(|C_{i\alpha}|^2 - |C_{i\beta}|^2)^2\gamma_i(0) \end{aligned} \quad (15)$$

The off-diagonal relaxation factors $\Gamma'_{\alpha\beta}$ for models II and III are given in Table 2. It is noted that $\Gamma'_{\alpha\beta}$ vanishes for model I due to $g_i = 0$ cm^{-1} (non-exciton−phonon coupling case). The magnitude of $\Gamma'_{\alpha\beta}$ is shown to be much larger than those in diagonal relative relaxation factor given in Table 1. From eq 15, $\Gamma'_{\alpha\beta}$ is turned out to be associated with the relative exciton distributions between states α and β. For example, $\Gamma'_{\alpha\beta}$ becomes small in the case of similar exciton distributions between two states, while for mutually different distributions the nonlocal exciton distributions tend to reduce $\Gamma'_{\alpha\beta}$. Such structure dependence of $\Gamma'_{\alpha\beta}$ via relative exciton distributions will be useful for understanding and controlling the NLO spectra for highly structure controlled dendritic systems. $\Gamma'_{\alpha 1}$ is also predcited to be large in lower exciton states because lower exciton states are composed of smaller number of monomers and then $\sum_i^N|C_{i\alpha}|^4$ ($\alpha \neq 1$) becomes larger than the case of higher exciton states.

TABLE 2: Pure Dephasing Factors $\Gamma'_{\alpha\beta}$ [cm^{-1}] for Models II (a) and III (b)

β	$\alpha = 7$	$\alpha = 6$	$\alpha = 5$	$\alpha = 4$	$\alpha = 3$	$\alpha = 2$
			(a) $g_i = 200$ cm^{-1}			
6	199.35					
5	248.86	248.86				
4	89.08	89.08	236.15			
3	97.18	97.18	244.46	154.16		
2	179.94	179.94	328.81	243.28	193.43	
1	245.51	245.51	394.70	232.80	241.11	325.46
			(b) $g_i = 1000$ cm^{-1}			
6	996.74					
5	1244.32	1244.32				
4	445.40	445.41	1180.74			
3	485.92	485.92	1222.30	770.81		
2	899.70	899.69	1644.04	1216.42	967.13	
1	1227.56	1227.57	1973.52	1163.99	1205.55	1627.28

3.3. Spatial Contributions of Excitons to Imaginary γ Peaks. Figure 5 shows the spatial contributions of excitons (see explanations below eq 10) to imaginary γ spectra for these three-photon resonance peaks for models I, II, and III, which are concerned with the exciton states **2**, **4** and **7**, respectively. In all cases, two-exciton contributions tend to be more delocalized

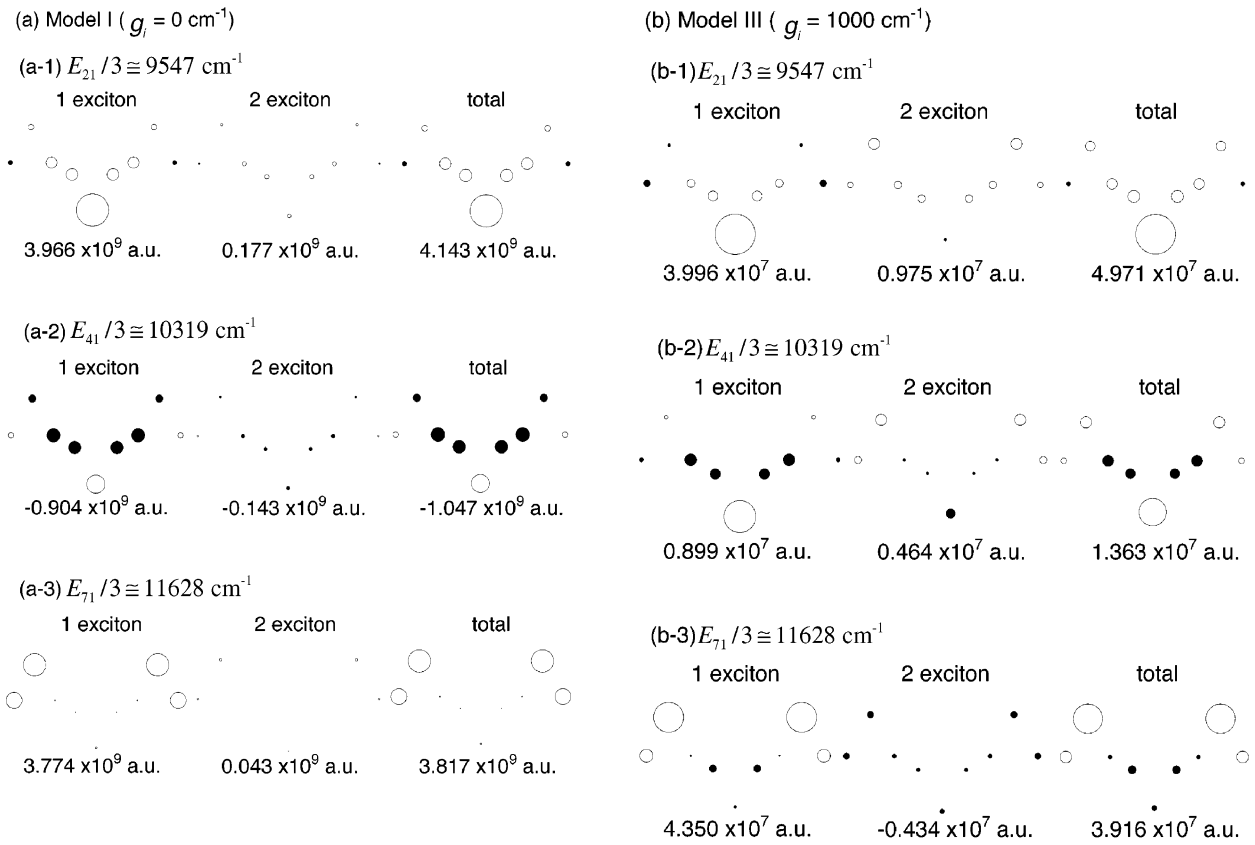

Figure 5. One, two, and total exciton spatial contributions to three imaginary γ peaks [(1) $E_{21}/3$ ($\cong$ 9547 cm^{-1}), (2) $E_{41}/3$ ($\cong$ 10319 cm^{-1}), and (3) $E_{71}/3$ ($\cong$ 11628 cm^{-1})] for models I (a) and III (b). White and black circles represent positive and negative values of contributions to γ, respectively.

over different generations than the one-exciton contributions though the two-exciton contributions are smaller than the one-exciton contributions. This can be understood by the fact that two-exciton contribution is described by the slight excitation over two different sites due to the one-photon off-resonant electric field. It is turned out form model I that the spatial contributions of each peak, a-1 at $E_{21}/3$ ($\cong$ 9547 cm^{-1}), a-2 at $E_{41}/3$ ($\cong$ 10319 cm^{-1}), and a-3 at $E_{71}/3$ ($\cong$ 11628 cm^{-1}) (see Figure 4), reflect the exciton distribution of states **2**, **4** and **7**, respectively. In comparison of the results for models I and III, the exciton relaxation effect tends to overlap these distinct spatial contributions with each other in addition to the significant reduction of the amplitude of the contribution primarily caused by the pure dephasing. In fact, the spatial contribution of total exciton at the first imaginary peak (b-1) for model III is shown to have the relative spatial distribution similar to the first imaginary peak (a-1) with a small mixing of the second imaginary peak (a-2) for model I though the magnitudes of peaks b for model III are much smaller than those of peaks a for model I. The exciton spatial contributions at the third imaginary peak (b-3) for model III is predicted to be constructed from a-3 with a small mixing of a-2 for model I. In particular, the second imaginary peak (b-2) for model III is shown to be significantly affected by the overlap of the neighboring large imaginary peaks a-1 and a-3 at the second imaginary peak position for model I. It is further found that the relative contribution of two-exciton generation with more spatially delocalized distributions to γ more enhances in model III than in model I (see, for example, a-2 and b-2). Such a feature is attributed to the relative increase in the virtual excitation processes involving two exciton states due to the pure dephasing caused by exciton relaxation effects originating in exciton−phonon coupling.[35]

4. Concluding Remarks

In this study, we have investigated the THG γ spectrum in the three-photon off- and on-resonant regions for nanostar dendritic aggregate systems including exciton relaxation effects. First, the qualitative feature of γ spectrum is found to be drastically changed for nanostar dendritic aggregate systems with dipole−dipole interaction as compared to that without dipole−dipole interactions. This change stems from the energy splitting by dipole−dipole interaction. The second change is caused by the exciton relaxation effects between states (originating in exciton−phonon coupling), which composed of exciton migration (diagonal) and pure-dephasing (off-diagnoal) parts. Since the pure dephasing parts are larger than the exciton migration parts, the broadening of γ spectrum for nanostar dendritic systems primarily originate in the pure dephasing parts of exciton relaxation. The pure dephasing parameter $\Gamma'_{\alpha\beta}$ between exciton state α and β is found to be closely related to the relative exciton distributions between the two states. It is also found that the spatial contributions to γ for high(low)-lying imaginary peak mainly come from the exciton distributions in the periphery (internal) region, while the exciton relaxation leads to the mutual overlap of spatial contributions to γ between neighboring peaks and the relative increase in the two-exciton spatial contributions. These features are shown to delocalize the spatial contributions of excitons, reducing the distinctiveness of spatial contribution to each peak. Such delocalization in spatial exciton contributions to γ is a contrast to the migration of exciton distribution, which is concentrated in the internal and core region in the stationary region. In conclusion, the exciton relaxation originating in exciton−phonon coupling is indispensable for investigating dynamic nonlinear optical properties of meso- and macroscopic supramolecular systems exhibiting exciton migration. These results also suggest that the possibility of mutual control of γ spectrum and energy migration by modifying the architecture of dendritic systems.

Acknowledgment. This work was supported by Grant-in-Aid for Scientific Research (No. 14340184) from Ministry of Education, Science, Sports and Culture, Japan.

References and Notes

(1) Knox, R. S. In *Primary Processes of Photosynthesis*; Barber, J., Ed.; Elsevier, Amsterdam, 1977; Vol. 2.
(2) Deming-Adams, B. *Biochim. Biophys. Acta* **1990**, *1*, 1020.
(3) Valkunas, L.; Geacintov, N. E.; France, L. L. *J. Lumin.* **1992**, *51*, 67.
(4) Archut, A.; Azzellini, G. C.; Balzani, V.; De Cola, L.; Vögtle, F. *J. Am. Chem. Soc.* **1998**, *120*, 12187.
(5) Brédas, J. L.; Beljonne, D.; Coropceanu, V.; Cornil, J. *Chem. Rev.* **2004**, *104*, 4971.
(6) Coropceanu, V.; Gruhn, N.; Barlow, S.; Lambert, C.; Durivage, J.; Bill, T.; Noell, G.; Marder, S. R.; Brédas, J. L. *J. Am. Chem. Soc.* **2004**, *126*, 2727.
(7) Pond, S. J. K.; Tsutsumi, O.; Rumi, M.; Kwon, O.; Zojer, E.; Brédas, J. L.; Marder, S. R.; Perry, J. W. *J. Am. Chem. Soc.* **2004**, *126*, 9291.
(8) Jones, S. C.; Coropceanu, V.; Barlow, S.; Kinnibrugh, T.; Timofeeva, T.; Brédas, J. L.; Marder, S. R. *J. Am. Chem. Soc.* **2004**, *126*, 11782.
(9) Rumi, M.; Ehrlich, J. E.; Heikal, A. A.; Perry, J. W.; Barlow, S.; Hu, Z.; McCord-Maughon, D.; Parker, T. C.; Rkel, H.; Thayumanavan, S.; Marder, S. R.; Beljonne, D.; Brédas, J. L. *J. Am. Chem. Soc.* **2000**, *122*, 9500.
(10) Buhleier, E.; Wehner, W.; Vögtle, F. *Synthesis* **1978**, *155*.
(11) Hawker, C.; Fréchet, J. M. J. *J. Am. Chem. Soc.* **1990**, *112*, 7638.
(12) Fréchet, J. M. J. *Science* **1994**, *263*, 1710.
(13) Fischer, M.; Vögtle, F. *Angew. Chem., Int. Ed. Engl.* **1999**, *38*, 884.
(14) Bosman, A. W.; Janssen, H. M.; Meijer, E. W. *Cem. Rev.* **1999**, *99*, 1665.
(15) Reinhoudt, D. N., Ed.; *Supramolecular Materials and Technologies*, *Perspectives in Supramolecular Chemistry*; Wiley: New York, 1999; Vol. 4.
(16) Kleiman, V. D.; Melinger, J. S.; McMorrow, D. *J. Phys. Chem. B* **2001**, *105*, 5595.
(17) Nakano, M.; Yamaguchi, K. Polarizabilities and hyperpolarizabilities of dendritic systems. In *Advances in Multiphoton Processes and Spectroscopy 15*; World Scientific: Singapore, 2003; p 1.
(18) Nakano, M.; Fujita, H.; Takahata, M.; Yamaguchi, K. *J. Am. Chem. Soc.* **2002**, *124*, 9648.
(19) (a) Nakano, M.; Fujita, H.; Takahata, M.; Yamaguchi, K. *J. Chem. Phys.* **2001**, *115*, 1052 (b) Nakano, M.; Fujita, H.; Takahata, M.; Yamaguchi, K. *J. Chem. Phys.* **2001**, *115*, 6780.
(20) Nakano, M.; Kishi, R.; Takahata, M.; Nitta, T.; Yamaguchi, K. *J. Lumin.* **2005**, *111*, 359.
(21) Xu, Z.; Moor, J. S. *Acta Polym.* **1994**, *45*, 83.
(22) Devadoss, C.; Bharathi, P.; Moore, J. S. *J. Am. Chem. Soc.* **1996**, *118*, 9635.
(23) Shortreed, M. R.; Swallen, S. F.; Shi, Z.-Y.; Tan, W.; Xu, Z.; Devadoss, C.; Moore, J. S.; Kopelman, R. *J. Phys. Chem. B* **1997**, *101*, 6318.
(24) Kopelman, R.; Shortreed, M.; Shi, Z.-Y.; Tan, W.; Bar-Haim, A.; Klafter, J. *Phys. Rev. Lett.* **1997**, *78*, 1239.
(25) Bar-Haim, A.; Klafter, J.; Kopelman, R. *J. Am. Chem. Soc.* **1997**, *26*, 66197.
(26) Tretiak, S.; Chernyak, V.; Mukamel, S. *J. Phys. Chem. B* **1998**, *102*, 3310.
(27) Kirkwood, J. C.; Scheurer, C.; Chernyak, V.; Mukamel, S. *J. Chem. Phys.* **2001**, *114*, 2419.
(28) Tretiak, S.; Mukamel, S. *Chem. Rev.* **2002**, *102*, 3171.
(29) Nakano, M.; Takahata, M.; Fujita, H.; Kiribayashi, S.; Yamaguchi, K.; *Chem. Phys. Lett.* **2000**, *323*, 249.
(30) Takahata, M.; Nakano, M.; Fujita, H.; Yamaguchi, K. *Chem. Phys. Lett.* **2002**, *363*, 422.
(31) Takahata, M.; Nakano, M.; Yamaguchi, K. *J. Theor. Comput. Chem.* **2003**, *2*, 459.
(32) Nakano, M.; Takahata, M.; Yamada, S.; Yamaguchi, K.; Kishi, R.; Nitta, T. *J. Chem. Phys.* **2004**, *120*, 2359.
(33) Carmichael, H. J. *Statistical Methods in Quantum Optics 1*; Springer, Verlag: Berlin 1999.
(34) Nakano, M.; Yamaguchi, K. *Phys. Rev. A* **1994**, *50*, 2989.
(35) Dick, B.; Hochstrasser, R. M.; Trommsdorff, H. P. *Nonlinear optical properties of organic molecules and crystals*; AT&T: New York, 1987; Vol. 2, p 159.